STEREOTACTIC RADIOTHERAPY OF PRIMARY LUNG CANCER AND OTHER TARGETS: RESULTS OF CONSULTANT MEETING OF THE INTERNATIONAL ATOMIC ENERGY AGENCY (*INT J RADIAT ONCOL BIOL PHYS* 2011;79:660–669)

To the Editor: We read with great interest the article by Nagata et al. (1) in which they nicely evaluated the current status of stereotactic body radiotherapy (SBRT) in developing countries and recommendations following the meeting of consultants of the International Atomic Energy Agency (IAEA). We very much appreciate their contribution, as their findings and experiences will have major implications for our clinical daily practice of SBRT treatment and planning in the developing world.

In their report, Nagata et al. advised using the minimum methodology, technology, and quality assurance requirements for SBRT in treating primary lung tumors and other body tumors. Patients who are candidates for SBRT for lung tumors are generally those whose cases are medically inoperable and have poor performance status, with cardiac or other comorbidities, and a significant number of those patients may present with implanted cardiac pacemakers (ICP). Such a report should also have discussed this potential problem. We would like to share our experience with and opinion regarding image-guided SBRT for early-stage lung cancer patients with ICP, in that respect.

Among our 25 SBRT lung patients treated since 2008, we treated a 76-year-old medically inoperable patient who was diagnosed with early-stage lung cancer, who had received an ICP in 2006. Total dose of 5,500 cGy was given in 5 fractions with our Trilogy linear accelerator-based system, with daily pre- and posttreatment kV-kV imaging and cone beam computerized tomography (CBCT) for image guidance. We reported this case, in which we followed the recommendations of the American Association of Physicists in Medicine Task Group report for treating this patient, which was published in 1994 (2). We limited the total dose to the ICP to less than 5 Gy and refrained from using direct beams through the ICP device. During treatment, an erratic pacing happened due to the transient interference, and this was retrospectively recorded by the ICP device memory analysis. No immediate severe side effect happened during SBRT. The patient had cardiac problems and expired 1 month after treatment. However, these cardiac problems were not found to be related to pacemaker malfunction.

Although the aforementioned task group report is available for management of ICP patients, this report was published in 1994. At that time, hypofractionated treatments with currently different kind of image guidance (like CBCT and kV-kV imaging) methods were not available. Therefore, more studies of the effect of high-dose hypofractionated treatments and new image guidance methods for ICPs are needed. In this important IAEA report, we believe that the information and warnings about managing patients with ICPs are lacking. Our colleagues dealing with these kinds of new treatment methods should be aware of this problem.

Banu Atalar, M.D.
Hale Caglar, M.D.
Department of Radiation Oncology
Acibadem University
Istanbul, Turkey

Enis Ozyar, M.D.
Institute of Health Sciences and Radiation Oncology Department
Acibadem University
Istanbul, Turkey

doi:10.1016/j.ijrobp.2011.06.1989

1. Nagata Y, Wulf J, Lax I, Timmerman R, Zimmermann F, Stojkovski I, Jeremic B. Stereotactic radiotherapy of primary lung cancer and other targets: Results of consultant meeting of the International Atomic Energy Agency. *Int J Radiat Oncol Biol Phys* 2011;79(3):660–669.
2. Marbach JR, Sontag MR, Van Dyk J, Wolbarst AB. Management of radiation oncology patients with implanted cardiac pacemakers: report of AAPM Task Group No. 34. American Association of Physicists in Medicine. *Med Phys* 1994;21(1):85–90.

IN REPLY TO DRS. ATALAR, CAGLAR, AND OZYAR

To the Editor: We thank Drs. Atalar, Caglar, and Ozyar for their comments on stereotactic body radiotherapy (SBRT) for a patient with implanted cardiac pacemakers (ICPs). They reported on 1 patient who died 1 month after SBRT with cardiac problems probably unrelated to RT. However, they suggested the establishment of a new guideline for ICPs and implantable cardioverter defibrillators (ICDs) in the era of SBRT and image-guided RT.

Our nation-wide survey conducted by the Japan Conformal External Beam Radiotherapy Group (J-CERG) did not include any patients who died after SBRT with malfunction of ICPs and ICDs (1).

When a tumor was situated at the same level of the ICP, the computed tomography image of the ICP would be accompanied by severe metallic artifacts. These computed tomography images are not suitable for SBRT planning. Even in such a case, SBRT can be indicated when the position of the subcutaneous ICP can be changed by the patient raising their hands upward.

A direct radiation beam through the ICP should be avoided. Also, when a tumor is situated just below the chest wall of the ICP, I would recommend the cardiologists to replace the ICP to an abdominal position.

Another Japanese prospective survey of patients with ICP and ICD found 1 case of malfunction in a patient with prostate cancer treated by intensity-modulated RT to the prostate. Even when the ICP is not situated at the same tumor level and no beam passes through the ICP, they recommended precautions during the planning and administration of RT (2).

In conclusion, I advise a direct beam path through ICP should be avoided in the case of SBRT. Moreover, all radiation oncologists should ask a medical engineering officer to check the ICP before and after SBRT because of the data reported by several studies on the usual RT for patients with an ICP/ICD (3–5).

Yasushi Nagata, M.D.
Department of Radiation Oncology
Hiroshima University
Hiroshima, Japan

doi:10.1016/j.ijrobp.2011.06.1993

1. Nagata Y, Hiraoka M, Mizowaki T, *et al.* Survey of stereotactic body radiation therapy in Japan by the Japan 3-D Conformal External Beam Radiotherapy Group. *Int J Radiat Oncol Biol Phys* 2009;75:343–347.
2. Soejima T, Yoden E, Nishimura Y, *et al.* Radiation therapy in patients with implanted cardiac pacemakers and implantable cardioverter defibrillators: A prospective survey in Japan. *J Radiat Res* 2011;52:516–521.
3. Hurkmans CW, Sceppers E, Springorum BGF, *et al.* Influence of radiotherapy on the latest generation of implantable cardioverter-defibrillators. *Int J Radiat Oncol Biol Phys* 2005;63:282–289.
4. Gelblum DY, Amols H. Implanted cardiac defibrillator care in radiation oncology patient population. *Int J Radiat Oncol Biol Phys* 2009;73:1525–1531.
5. Solan AN, Solan MJ, Bednarz G, *et al.* Treatment of patients with cardiac pacemakers and implantable cardioverter-defibrillators during radiotherapy. *Int J Radiat Oncol Biol Phys* 2004;59:897–904.

RESPONSE TO "THE PHYSICS AND TECHNOLOGY OF RADIATION THERAPY BOOK REVIEW" (*INT J RADIAT ONCOL BIOL PHYS* 2011;80:637

To the Editor: We thank Dan Odero for his review of our book *The Physics and Technology of Radiation Therapy* in the June 2011 issue (1). When reviewing an 850-page book, it is usually not practical to read the entire volume. We believe that this has led to some misunderstandings. We have been criticized for leaving some things out of the book that are, in fact, in the book. Regarding the reference to the "Mevalac" linear accelerator (linac), we are criticized because "there exists no such linac or manufacturer." The book clearly and repeatedly states (on Pages 12.5, 15.2, 15.5, and 15.23, as well as in the index [Page I.10]) that this is a fictitious linac. We give detailed dosimetry data for this fictitious machine in Appendix C. The title page to the appendix again states that this is a fictitious linac. It is stated that radiochromic dosimetry is not mentioned, yet this topic is discussed on Page 8.33. Regarding the use of thermoluminescent dosimeters for "external agency machine output verification," if this is referring to the RPC mailed dosimetry program, the RPC no longer uses thermoluminescent dosimeters. This is discussed in Chapter 11 (Page 11.13). Dr. Odero states that the physician reader needs to understand the importance of positron decay and electron capture, particularly for ^{125}I and ^{103}Pd. The decay of ^{125}I

Technical Report

Coronary Artery Calcium Scoring on Different 64-detector Scanners Using a Low-tube Voltage (80 kVp)

Chikako Fujioka, PhD, Yoshinori Funama, PhD, Masao Kiguchi, RT, Minoru Ishifuro, PhD, Yasuki Kihara, MD, Yasushi Nagata, MD, Kazuo Awai, MD

Purpose: The aim of this study was to compare the calcium score and reproducibility of coronary artery calcium scores obtained on the four kinds of 64-detector computed tomography (CT) scanners using standard (120 kVp) and low tube voltage (80 kVp) scan techniques.

Materials and Methods: We scanned 80 and 120 kVp on all scanners. We calculated Agatston, volume, and mass scores for coronary artery calcium scoring on each scanner and compared the coefficients of variation of the calcium scores to evaluate reproducibility of among CT scanners.

Results: The averages of the total mean Agatston score, total mean volume score, and total mean mass score at 80kVp/120kVp were 798.9/683.8, and 627.2/567.3, and 157.1/156.7, respectively. The total mean mass score was almost constant irrespective of the tube voltage. The total mean coefficients of variation for the four CT scanners were lower at 80 than 120 kVp (4.1% vs. 10.2% [total mean Agatston score], 3.2% vs. 9.6% [total mean volume score], and 3.2% vs. 9.4% [total mean mass score]).

Conclusion: Use of the low tube voltage technique can reduce variations in the coronary artery calcium scores obtained on different CT scanners.

Key Words: Cardiac CT; coronary artery calcium score; MDCT; low tube voltage; heart.

Coronary artery calcium scoring by cardiac computed tomography (CT) is a reliable diagnostic tool in patients with suspected coronary artery disease because the degree of coronary calcification is strongly associated with the degree of atherosclerosis (1–4). The coronary artery calcium score on screening CT images yields relevant prognostic information on the development of coronary events (5–7). Although coronary artery calcium scoring was devised originally for electron beam CT by Agatston (1), it is now widely performed on multidetector CT (MDCT). For follow-up studies of patients with coronary artery disease, the use of the same CT scanner is desirable from the perspective of reproducibility among different CT scanners. However, this is not always possible and follow-up studies are often performed on different scanners.

The CT number of a scanned object depends on the effective tube voltage. Individual CT scanners have a specific effective tube voltage that corresponds to the "nominal" kilovolts peak (kVp). Consequently, different CT scanners yield different CT numbers even if the same object is scanned at the same kVp. Calcium attenuation increases as the effective tube voltage decreases (8). We hypothesized that variations in coronary artery calcium scores obtained on different CT scanners may be mitigated by increasing the signal intensity of calcium by using a low tube voltage technique. Although the image noise level is the same at 120 kVp and 80 kVp, because of the increased signal intensity at 80 kVp, coronary artery calcium can be certainly detected on scans acquired at 80 kVp. Therefore, the purpose of this study was to compare the calcium score and reproducibility of coronary artery calcium scores obtained on different CT scanners using standard (120 kVp) and low tube voltage (80 kVp) scan techniques.

MATERIALS AND METHODS

Phantom

We used a cardiac CT calibration phantom (QRM, Moehrendorf, Germany; http://www.qrm.de) designed as a calibration standard for the quantification of coronary calcium (9) (Fig 1). The phantom is static without cardiac motion. It consists of two parts, an anthropomorphic phantom body and a calibration insert. The phantom body includes artificial lungs and a

Acad Radiol 2012; 19:1402–1407

From the Departments of Radiology (C.F., M.K., M.I., Y.N.), Cardiovascular Medicine (Y.K.), and Diagnostic Radiology (K.A.), Hiroshima University, 1-2-3 Kasumi-cho, Minami-ku, Hiroshima 734-8551, Japan; Department of Medical Information Systems, Faculty of Life Sciences, Kumamoto University, Kumamoto, Japan (Y.F.). Received January 7, 2012; accepted July 7, 2012. **Address correspondence to:** C.F. e-mail: fujioka@hiroshima-u.ac.jp

http://dx.doi.org/10.1016/j.acra.2012.07.003

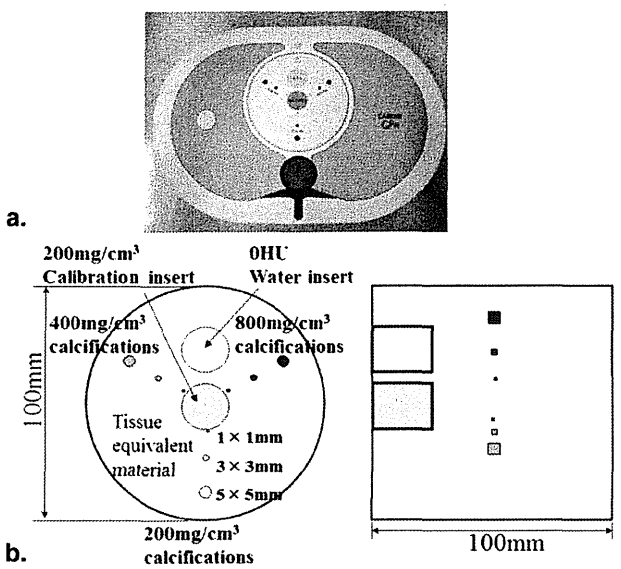

Figure 1. **(a)** Frontal view of the anthropomorphic phantom body with the calibration insert. **(b)** Diagrams of frontal (*left*) and side (*right*) views of the calibration insert with the nine different calcifications and the two large calibration inserts (Hounsfield units [HU] = 0, water and 200 mg/cm^3 calcium hydroxyapatite).

spine insert surrounded by material equivalent to soft tissue. The phantom is 300 mm in width (x-axis), 200 mm in anteroposterior diameter (y-axis), and 100 mm in length (z-axis). At the position of the heart there is a 100-mm-diameter cylindrical hole that permits placement of a calibration insert containing three series of calcified cylinders measuring 1.0, 3.0, and 5.0 mm in diameter and 1.0, 3.0, and 5.0 mm in height, respectively. The calcium hydroxyapatite (CaHA) density of each series of calcified cylinders equals 200, 400, and 800 mg/cm^3, respectively (Fig 1). In addition, the calibration insert contains 2 large homogeneous inserts. One of them is made of water equivalent material, the other one contains hydroxyapatite (CaHA density 200 mg/cm^3).

CT Scanning

We obtained prospectively-gated step-and-shoot scans on 64-detector CT scanners produced by 4 manufacturers (Aquilion64, Toshiba Medical Systems, Tokyo; LightSpeed VCT, GE Healthcare, Waukesha, WI; SOMATOM Definition AS +, Siemens Medical Systems, Erlangen, Germany; and Brilliance-64, Philips Medical Systems, Cleveland, OH). The scan parameters for obtaining the coronary artery calcium scores are shown in Table 1. We applied low (80 kVp) and standard tube voltage settings (120 kVp) on all scanners. For each CT scanner, we increased the tube current at 80 kV so that the image noise was at the same level (20 Hounsfield units [HU]) as at 120 kVp. Preliminary tube current values obtained at 120 and 80 kVp were based on image noise measurements of the water insert part in the phantom (Fig 1). Detailed scanner parameters including the tube current at 120 and 80 kVp are shown in Table 1. At each experiment, the phantom was scanned five times without being repositioned. Acquired data were reconstructed at 75% of the R-R interval; the nonoverlapping slice thickness was 3.0 or 2.5 mm; the field of view was 250 mm. We used the reconstruction kernel recommended by the manufacturer of the different scanners to acquire the coronary artery calcium scores (Table 1).

Analysis of Coronary Artery Calcium Scoring

We used Agatston, volume, and mass scores for coronary artery calcium scoring (1,10–12). Each score was calculated with the equation:

$$\text{Agatston score} = \text{slice increment/slice thickness} \times \sum (\text{area} \times \text{weighting factor}),$$

where the weighting factor = 1 if 130 HU $\leq CT_{max} <$ 200 HU, = 2 if 200 HU $\leq CT_{max} <$ 300 HU, = 3 if 300 HU $\leq CT_{max} <$ 400 HU, and = 4 if 400 HU $\leq CT_{max}$, the volume score $=\Sigma$ (area $\times$ slice increment), and the mass score $= \Sigma$ (area $\times$ slice increment $\times$ mean CT density) $\times$ calibration factor (12).

To calculate the Agatston, volume, and mass scores, the CT number threshold for 120 and 80 kVp was set at a default threshold of 130 HU (9). To obtain the calcium mass we calculated the calibration factor by measuring the attenuation of the large CaHA calibration insert at 200 mg/cm^3 and the water insert. The calibration factor c can be determined with the equation:

$$c = 200/(HU_{CaHA} - HU_{water}).$$

The circular regions of interest were of a 145 mm^2 area (Fig 2). The calibration factor was corrected for the different tube voltages and CT scanners. We calculated the calibration factor at each tube voltage and for each scanner (Table 1). The calibration factor describes the scanner-specific attenuation of calcium. It is necessary to derive the calcium mass from the mean attenuation and the measured volume of a lesion (12).

All reconstructed images were analyzed on a workstation (Virtual Place Raijin, AZE, Tokyo, Japan). One of the authors (C.F.), a radiological technologist with 14 years of experience in cardiac CT, measured calcifications 3.0 and 5.0 mm in size and 200, 400, and 800 mg/cm^3 in density by using a fixed 130-HU threshold, and calculated the Agatston, volume, and mass scores obtained on the four CT scanners at the two tube voltages. The smallest calcium inserts (1.0 mm in size and of all densities) were not assessed because their attenuation values (CT number) were below the threshold. Therefore, the known total mass score (167.1 mg) was computed from the total mass (168.22 mg)–1.12 mg of the 1.0 mm mass (9). The Agatston, volume, and mass scores were acquired five times from five scan data sets; the total mean score and standard deviation (SD) for 120 and 80 kVp were calculated from five data sets obtained with each CT scanner.

TABLE 1. Scan Parameters for Coronary Artery Calcium Scoring

	Scanner							
	Aquilion-64		Light Speed VCT		Definition AS+		Briliance-64	
Rotation time (sec)	0.25		0.35		0.217		0.28	
Tube voltage (kV)	120	80	120	80	120	80	120	80
Tube current (mA)	70	240	95	265	70	254	86	350
Calibration factor	0.70	0.51	0.71	0.51	0.83	0.59	0.81	0.56
Noise (mean ± SD)	21.0 ± 0.4	20.4 ± 0.8	19.9 ± 0.9	21.3 ± 0.6	20.6 ± 1.2	20.8 ± 0.5	19.9 ± 0.6	20.9 ± 1.0
CTDIw (mGy)	1.60	1.90	1.58	1.37	0.88	0.83	1.70	2.10
Detector configuration (mm)	64 × 0.5		64 × 0.625		64 × 0.6		64 × 0.625	
Section thickness (mm)	3.0		2.5		3.0		2.5	
Table feed (mm/rotation)	32.0		40.0		38.4		40.0	
Beam pitch	1		1		1		1	
Reconstruction kernel	FC13		Standard		B35f Heart View medium		Cardiac Standard	

CTDIw, weighted computed tomography dose index.

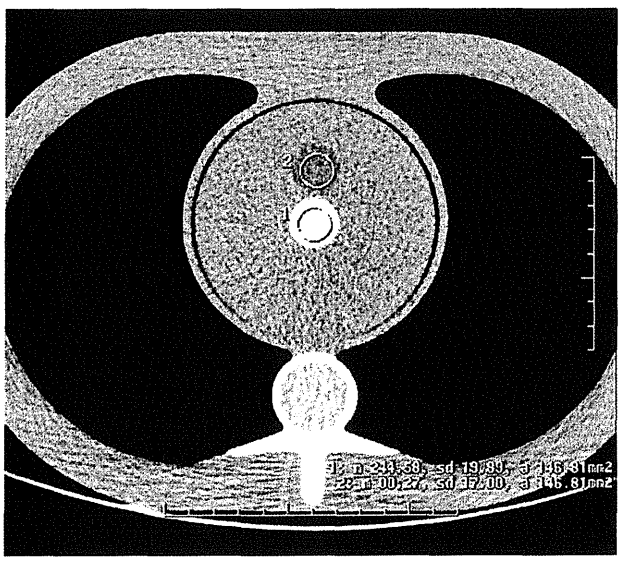

Figure 2. Transverse computed tomography (CT) images of the semianthropomorphic thoracic phantom. To determine the mean CT numbers, circular regions of interest (mean area 145 ± 1.0 mm^2) were used for the calibration factor.

We also calculated the coefficients of variation for each CT scanner using the equation:

$$\text{coefficient of variation} = 100 \times [\text{standard deviation}]/\text{mean} \quad (9)$$

Statistical Analysis

We used Kruskal-Wallis one-way analysis of variance on ranks to compare each Agatston, volume, and mass score acquired at 120 and 80 kV on the four different CT scanners. When the overall differences were statistically significant we performed post-hoc analysis using the Steel-Dwass multiple comparison test. Differences of $P < .05$ were considered statistically significant. Calculation of Kruskal-Wallis one-way analysis of variance was with a statistical software program (MedCalc Software; MedCalc, Mariakerke, Belgium). Calculation of the Steel-Dwass multiple comparison test was with a commercially available software program (Statcel3, Saitama, Japan).

RESULTS

The Agatston, volume, and mass scores at 80 and 120 kVp for the four different scanners are shown in Tables 2A and 2B. The data for each size are presented as the sum of different calcium density values ranging from 200 to 800 mg/cm^3. At 120 kVp, the total mean and standard deviation of the total mean Agatston, volume, and mass scores obtained on the four CT scanners was 683.8 ± 69.7, 567.3 ± 54.6, and 156.7 ± 14.7, respectively (Table 2A). There were large variations and statistically significant differences in the total Agatston score between the Aquilion-64 and the Brilliance-64 instrument ($P < .05$). With respect to the mass score, there was a statistically significant difference between all pairs of CT scanners ($P < .05$). When we excluded the Brilliance-64 scanner, we found that at 120 kVp, the total mean and standard deviation of the total mean Agatston, volume, and mass scores were higher (ie, 717.2 ± 23.9, 593.6 ± 17.2, and 163.9 ± 2.8, respectively).

At 80 kVp, the mean coronary artery calcium scores were 798.9 ± 32.4, 627.2 ± 20.1, and 157.1 ± 5.1 (Table 2B). The total mean Agatston and total mean volume scores were 16.8% and 10.6% higher at 80 than 120 kVp, respectively; the total mean mass scores were almost the same at 80 and 120 kVp. At 80 kVp, we observed stable variations among the different CT scanners in the total mean Agatston, volume, and mass scores, irrespective of the inclusion or exclusion of the Brilliance-64 instrument. In addition, comparison of data acquired at 120 kVp and 80 kVp on the same CT scanner showed that the standard deviation for the Agatston, volume, and mass scores was almost the same or lower at 80 kVp. Coefficient of variation (%) obtained with different CT scanners are shown in Tables 3. At all CT scanners, the coefficient of variation (%) were lower at 80 than 120 kVp. The total

TABLE 2A. Mean Coronary Artery Calcium Scores Obtained at 120 kVp

	Scanner				All Scanners	The Three Vendors (excluding Brilliance-64)
Score	Aquilion-64	Light Speed VCT	Definition AS+	Briliance-64	Average ± SD	Average ± SD
Agatston						
Total	744.8 ± 65.8	704.4 ± 57.2	702.5 ± 51.1	583.4 ± 61.8	683.8 ± 69.7	717.2 ± 23.9
3 mm	148.6	140.5	127.7	101.1	129.5 ± 20.8	138.9 ± 10.5
5 mm	596.2	563.9	574.8	482.3	554.3 ± 49.9	578.3 ± 16.5
volume (mm^3)						
Total	611.4 ± 34.1	577.1 ± 29.2	592.4 ± 26.3	488.2 ± 44.6	567.3 ± 54.6	593.6 ± 17.2
3 mm	129.3	116.3	112.0	88.3	111.5 ± 17.1	119.2 ± 9.0
5 mm	482.1	460.7	480.4	399.8	455.8 ± 38.5	474.4 ± 11.9
Mass (mg)						
Total	163.8 ± 4.1	161.2 ± 1.6	166.8 ± 3.2	134.9 ± 10.1	156.7 ± 14.7	163.9 ± 2.8
3 mm	27.1	27.3	26.6	20.7	25.4 ± 3.2	27.0 ± 0.4
5 mm	136.6	133.9	140.2	114.2	131.2 ± 11.7	136.9 ± 3.2

* Steel-Dwass test, $P < .05$.

TABLE 2B. Mean Coronary Artery Calcium Scores Obtained at 80 kVp

	Scanner				All Scanners	The Three Vendors (excluding Brilliance-64)
Score	Aquilion-64	Light Speed VCT	Definition AS+	Briliance-64	Average ± SD	Average ± SD
Agatston						
Total	845.0 ± 44.9	792.0 ± 49.8	769.1 ± 32.1	789.7 ± 53.0	798.9 ± 32.4	802.0 ± 38.9
3 mm	160.9	156.4	148.3	156.5	155.5 ± 5.2	155.2 ± 6.4
5 mm	684.1	635.6	620.8	633.2	643.4 ± 27.9	646.8 ± 33.1
volume (mm^3)						
Total	652.4 ± 41.0	607.7 ± 27.1	614.8 ± 21.0	633.7 ± 39.7	627.2 ± 20.1	625.0 ± 24.0
3 mm	132.9	125.5	120.7	129.6	127.2 ± 5.2	126.4 ± 6.1
5 mm	519.5	482.2	494.1	504.1	500.0 ± 15.8	498.6 ± 19.1
Mass (mg)						
Total	161.8 ± 4.2	154.2 ± 1.8	161.0 ± 1.4	151.4 ± 9.7	157.1 ± 5.1	159.0 ± 4.2
3 mm	26.2	26.1	25.7	25.1	25.8 ± 0.5	26.0 ± 0.3
5 mm	135.6	128.1	135.3	126.4	131.4 ± 4.8	133.0 ± 4.3

* Steel-Dwass test, $P < .05$.

mean coefficients of variation for the four CT scanners were lower at 80 than 120 kVp (4.1% vs. 10.2% [total mean Agatston score], 3.2% vs. 9.6% [total mean volume score], and 3.2% vs. 9.4% [total mean mass score]).

DISCUSSION

Our coefficients of variation for Agatston, volume, and mass scores were similar to those reported by others. According

TABLE 3. Coefficient of Variation (%) Obtained with Different CT Scanners

		Scanner			
Score	kVp	Aquilion-64	Light Speed VCT	Definition AS+	Briliance-64
Agatston	120	8.8	8.1	7.3	10.6
	80	5.3	6.3	4.2	6.7
Volume (mm^3)	120	5.6	5.1	4.4	9.1
	80	6.3	4.5	3.4	6.3
Mass (mg)	120	2.5	1.0	1.9	7.5
	80	2.6	1.2	0.9	6.4

to McCollough et al (9), at 120 kVp they were 4.0%, 7.9%, and 4.7%; in another study (13) the coefficients of variation for volume scores at 120 kVp were 3.2%–10.3%. We found that these values were smaller at 80 than 120 kVp. The CT number of smaller and lower density calcifications may be more easily affected by the partial volume effect. As the CT number of calcifications is increased at 80 kVp, smaller, lower density calcifications may be more accurately identified on 80 than 120 kVp scans and the coefficients of variation for the calcium scores may be smaller at 80 than 120 kVp. Although the coefficients of variation for each calcium score were smaller at 80 than 120 kVp, the absolute value of the Agatston and volume scores were higher at 80 kVp. In the clinical setting, the commonly used tube voltage is 120 kVp and the calcium score obtained at 80 kVp may overestimate the degree of arteriosclerosis. Therefore, a standard for calcium scores obtained at 80 kVp is needed.

Because Agatston scores are significant predictors of events in patients with coronary heart disease, they are widely used in the clinical setting. Although the scoring system has several limitations, a large amount of data acquired and analyzed by using Agatston scores is already available. However, the Agatston score depends strongly on noise because it is based on maximum CT numbers. Therefore, we recommend use of the mass score for evaluating coronary artery calcification because it was almost the same on 120 and 80 kVp scans and the coefficients of variation were small at both 120 and 80 kVp. As the value of the mass score is corrected with the calibration factor, we posit that it can be used to estimate the amount of calcification more accurately than other calcium scoring methods. The usefulness of the mass score has been reported (9,12,14). According to Hong et al (12), the calcium mass as a quantitative index for the amount of calcium yields more precise information than other methods because the pixels that compose each calcified lesion are corrected by an appropriate calibration factor to compensate for decreased mean CT numbers. They concluded that calcium mass measurements were more accurate and less variable. Thomas et al (14) also reported the advantage of calcium scoring at low tube voltage. They used the same scanner and 80 and 120 kVp to compare the Agatston, volume, and mass scores and concluded that an 80-kVp protocol allows for a dose reduction without compromising reproducibility and accuracy. In clinical situations, variations in coronary artery calcium score are greater than in phantom studies. Yoon et al (11) reported that the percentage differences in Agatston, volume, and mass scores were 37.2%, 28.2%, and 28.4% in clinical situations. On the other hand, according to others (10,15–17), the percentage difference in Agatston and volume scores was 25.5%–38.6% and 22.0%–30.0%, respectively, in phantom studies. This difference may be attributable to motion artifacts and the instability of the image noise level in clinical settings. With respect to motion artifacts, Braown et al reported that increasing motion time during image acquisition results in an apparent increase in the Agatston coronary artery calcium score (18). In addition, the pseudo-mass located close to the area of a lesion is strongly affected by motion artifacts (19). The slice thickness is also important factor in the acquisition of accurate calcium scores. To avoid the partial volume effect, thinner slices should be used. Vliegenthart et al (13), who compared the results obtained with 3.0- and 1.5-mm-thick slices, suggested that the partial volume effect on 3.0-mm-thick images may result in an underestimation of the calcium volume. Our slices were 3.0 mm or 2.5 mm in thickness, and the use of 1.5-mm thick images might improve calcium volume effect. On the other hand, the use of thinner slices might increase image noise and higher x-ray doses may be required to compensate for the increased noise. The scan starting position, table movement, and displacement of the phantom on the table also highly influence calcium measurements (19). In addition, the helical trajectory of the x-ray source is different at each repeat scan and may affect the calcium measurements because half-scan reconstruction is employed at cardiac scanning. Therefore, we scanned the phantom 5 times and computed the average score from the five scans for each scanner.

Our study has some limitations. First, as we used a static phantom free of cardiac motion, our findings did not consider the effect of cardiac motion artifact and varying heart rates. Our experimental results obtained with the phantom require validation in humans. In the next stage of our investigation, we will perform a multicenter study of coronary artery calcium scoring to compare the effects of factors such as motion artifact, patient size, and heart rate at 80 kVp and 120 kVp. Second, calcium scoring was performed on the same workstation to control for calculation errors

among different workstations. If different workstations are used for different scanners, the scores may differ slightly. Third, we applied the same weighting factor to correct the Agatston score at both 120 and 80 kVp. Considering the increase in the CT number at 80 kVp, the weighting factor at the 80 kVp voltage setting may need to be changed. Finally, we selected 64-detector scanners from four different vendors that are widely used for clinical examinations. If different scanners were employed, we may have observed changes in the reproducibility of data and in the observed variations. Nonetheless, we posit that on different scanners, there is a similar trend with respect to reproducibility and variations at 120 kVp and 80 kVp.

In conclusion, variations in coronary artery calcium scoring among different CT scanners can be reduced by the application of 80 kVp. Coronary artery calcium scoring at low tube voltage (80 kVp) provides for high reproducibility.

REFERENCES

1. Agatston AS, Janowitz WR, Hildner FJ, et al. Quantification of coronary artery calcium using ultrafast computed tomography. J Am Coll Cardiol 1990; 15:827–832.
2. Wexler L, Brundage B, Crouse J, et al. Coronary artery calcification: pathophysiology, epidemiology, imaging methods, and clinical implications. A statement for health professionals from the American Heart Association. Writing Group. Circulation 1996; 94:1175–1192.
3. Guerci AD, Spadaro LA, Goodman KJ, et al. Comparison of electron beam computed tomography scanning and conventional risk factor assessment for the prediction of angiographic coronary artery disease. J Am Coll Cardiol 1998; 32:673–679.
4. Rumberger JA, Sheedy PF, Breen JF, et al. Electron beam computed tomographic coronary calcium score cutpoints and severity of associated angiographic lumen stenosis. J Am Coll Cardiol 1997; 29:1542–1548.
5. Janowitz WR, Agatston AS, Kaplan G, et al. Differences in prevalence and extent of coronary artery calcium detected by ultrafast computed tomography in asymptomatic men and women. Am J Cardiol 1993; 72:247–254.
6. Arad Y, Spadaro LA, Goodman K, et al. Predictive value of electron beam computed tomography of the coronary arteries. 19-month follow-up of 1173 asymptomatic subjects. Circulation 1996; 93:1951–1953.
7. Detrano RC, Wong ND, Doherty TM, et al. Prognostic significance of coronary calcific deposits in asymptomatic high-risk subjects. Am J Med 1997; 102:344–349.
8. Nakayama Y, Awai K, Funama Y, et al. Abdominal CT with low tube voltage: preliminary observations about radiation dose, contrast enhancement, image quality, and noise. Radiology 2005; 237:945–951.
9. McCollough CH, Ulzheimer S, Halliburton SS, et al. Coronary artery calcium: a multi-institutional, multimanufacturer international standard for quantification at cardiac CT. Radiology 2007; 243:527–538.
10. Callister TQ, Cooil B, Raya SP, et al. Coronary artery disease: improved reproducibility of calcium scoring with an electron-beam CT volumetric method. Radiology 1998; 208:807–814.
11. Yoon HC, Greaser LE, 3rd, Mather R, et al. Coronary artery calcium: alternate methods for accurate and reproducible quantitation. Acad Radiol 1997; 4:666–673.
12. Hong C, Bae KT, Pilgram TK, et al. Coronary artery calcium measurement with multi-detector row CT: in vitro assessment of effect of radiation dose. Radiology 2002; 225:901–906.
13. Vliegenthart R, Song B, Hofman A, et al. Coronary calcification at electron-beam CT: effect of section thickness on calcium scoring in vitro and in vivo. Radiology 2003; 229:520–525.
14. Thomas CK, Mühlenbruch G, Wildberger JE, et al. Coronary artery calcium scoring with multislice computed tomography: in vitro assessment of a low tube voltage protocol. Invest Radiol 2006; 41:668–673.
15. Wang S, Detrano RC, Secci A, et al. Detection of coronary calcification with electron-beam computed tomography: evaluation of interexamination reproducibility and comparison of three image-acquisition protocols. Am Heart J 1996; 132:550–558.
16. Yoon HC, Goldin JG, Greaser LE, 3rd, et al. Interscan variation in coronary artery calcium quantification in a large asymptomatic patient population. AJR Am J Roentgenol 2000; 174:803–809.
17. Greaser LE, Yoon HC, Mather RT, et al. Electron-beam CT: the effect of using a correction function on coronary artery calcium quantitation. Acad Radiol 1999; 6:40–48.
18. Brown SJ, Hayball MP, Coulden RA. Impact of motion artefact on the measurement of coronary calcium score. Br J Radiol 2000; 73: 956–962.
19. Dijkstra H, Greuter MJ, Groen JM, et al. Coronary calcium mass scores measured by identical 64-slice MDCT scanners are comparable: a cardiac phantom study. Int J Cardiovasc Imaging 2010; 26: 89–98.

Geminin Expression in Pancreatic Neuroendocrine Tumors

Possible New Marker of Malignancy

Masaki Aizawa, MD, Motohiro Kojima, MD, PhD,† Naoto Gotohda, MD, PhD,* Satoshi Fujii, MD, PhD,† Yuichiro Katoh, MD, PhD,* Takahiro Kinoshita, MD, PhD,* Shinichiro Takahashi, MD, PhD,* Masaru Konishi, MD, PhD,* Taira Kinoshita, MD, PhD,* and Atsushi Ochiai, MD, PhD†*

Objectives: We evaluated geminin labeling index (LI) as a new prognostic indicator of pancreatic neuroendocrine tumor.

Methods: Twenty-seven patients who underwent surgery were retrospectively referred. Labeling indices for geminin and Ki-67 were calculated and compared with clinicopathologic factors. Then, the concordance of positivity between 2 LIs was evaluated using the color difference quotation.

Results: The median (range) of LIs for geminin and Ki-67 was 1.0% (0.05%–14.9%) and 1.5% (0.02%–8.8%), respectively. When the high LI was defined as more than 2.0% according to the receiver operating characteristic curves determining the metastasis, both geminin LI (hazard ratio [HR], 31.382; 95% confidence interval [CI], 3.177–309.99; $P = 0.003$) and Ki-67 LI (HR, 6.182; 95% CI, 1.221–31.298; $P = 0.028$) were significant risk factors of recurrence in the univariate analysis. The Kaplan-Meier curves consistently exhibited the superiority of geminin LI (log rank, $P < 0.001$) to Ki-67 LI (log rank, $P = 0.041$) in predicting the disease-free survival. In the color difference quotation, the median ΔE of geminin stain (16.12; range, 5.8–41.9) was significantly larger than that of Ki-67 stain (13.17; range, 3.4–37.9).

Conclusions: The geminin LI was suggested to be more closely correlated with outcome and had more consistent positivity than the Ki-67 LI.

Key Words: geminin, neuroendocrine tumor, color difference quotation, prognostic factor, Ki-67

(*Pancreas* 2012;41: 512–517)

The annual incidence of pancreatic neuroendocrine tumor (PNET) is about 0.32 cases per population of 100,000 in the United States and 2.23 cases per population of 100,000 in Japan. Pancreatic neuroendocrine tumors are thought to represent 1%–2% of all pancreatic neoplasms. The apparent incidence and prevalence of PNET have increased substantially during the last 30 years, probably because of the rapid progress of innovative diagnostic techniques.[1] The best treatment for PNET is curative surgical resection, which has a disease-free survival rate of 82% after surgery.[2] Pancreatic neuroendocrine tumors have a wide spectrum of clinical presentations. Therefore, multiple studies have attempted to develop staging and grading systems to better define prognosis.[2–5] The 2000 World Health Organization (WHO) classification system used both stage-related criteria (size and presence of metastases) and grade-related criteria (mitotic rate, perineural invasion, angioinvasion, and Ki-67 proliferative index) to predict outcome. Though this approach included most well-accepted pathologic prognostic factors, the multiple grading parameters made it difficult to reproduce grades reliably among pathologists and institutions, and this grading system has since been replaced by the current WHO classification.[6] Immunohistochemistry for Ki-67 protein is commonly used to evaluate the proliferative activity of tumor cells, and numerous studies have shown that the labeling index (LI) of the Ki-67 protein is correlated with the clinical outcome of patients with a variety of malignant tumors, including PNET.[2,3,7–10] The Ki-67 protein is detected during all active cell cycle phases (G_1, synthesis, G_2, and mitosis and cytokinesis) but not in resting (G_0) cells, although its function remains uncertain.[11,12] Although histologic grade-based estimations of prognosis are extremely useful for interpreting biopsy samples, additional reliable markers are needed.

Geminin, a negative regulator of DNA replication, has recently been described as a novel marker of malignant potential.[13] During the G_1 phase, DNA replication is initiated by the recruitment of the origin recognition complex, composed of cell division cycle-6 and Cdt1, to specific points of replication origin in the genome; this recruitment, in turn, loads the minichromosome maintenance (Mcm) complex, which is composed of Mcm-2 to Mcm-7.[14] Geminin is specifically expressed during the S, G_2, and early M phases and interacts with Cdt1 to prevent the loading of the Mcm complex to points of origin that have already been initiated, thus ensuring a single replication per 1 cell cycle.[15,16] Geminin expression has been widely observed in various malignant neoplasms, and the number of geminin-positive cells is reportedly proportional to the cell proliferation index, as measured using Ki-67 expression.[13] High levels of geminin expression are reportedly correlated with a poorer clinical outcome in breast cancer,[17] renal cell carcinoma,[18] prostatic adenocarcinoma,[19] salivary gland carcinomas,[20] lung cancer,[21] and gastric hyperplasia.[22] However, the prognostic significance of geminin expression in PNET remains unknown.

The purpose of this study was to determine whether geminin expression defines the aggressiveness of PNET and to compare the clinical and diagnostic use of the geminin LI with that of the Ki-67 LI.

MATERIALS AND METHODS

Patients

Between 1994 and 2010, a total of 27 consecutive patients underwent primary surgical treatment for PNET at our institution. The medical records and surgical specimens of these patients were retrospectively examined in the present study.

From the *Division of Digestive Surgery and †Pathology Division, Research Center for Innovative Oncology, National Cancer Center Hospital East, Kashiwa, Japan.

Received for publication February 2, 2011; accepted September 23, 2011.

Reprints: Atsushi Ochiai, MD, PhD, Pathology Division, Research Center for Innovative Oncology, National Cancer Center Hospital East, 6-5-1 Kashiwanoha, Kashiwa, Chiba 277-8577, Japan (e-mail: aochiai@east.ncc.go.jp).

Dr Aizawa states no source of financial support and no disclosure of funding received for this work.

The authors declare no conflict of interest.

Patients with recurrent tumors were excluded. Follow-up clinical information was obtained from the patients' medical records. The follow-up time was measured from the date of surgery until disease-caused death or the end of the follow-up period.

Clinicopathologic Parameters

The grading and staging of each tumor were performed according to the WHO classification, the cancer staging manual of the American Joint Committee on Cancer (AJCC), and the classification proposed by the European Neuroendocrine Tumor Society (ENETS).[23,24]

The prognostic values of the following clinicopathologic parameters were examined in the present study: tumor diameter (<2 vs ≥2 cm), lymphatic or blood vessel infiltration (absent vs present), perineural invasion (absent vs present), serosal or retroperitoneal invasion (absent vs present), tumor extension beyond the pancreas (absent vs present), mitotic index per 10 high-power fields (10 HPFs) (<2 vs ≥2), regional and distant metastasis (absent vs present), and pathological stage (AJCC stage ≥ IIA vs AJCC stage ≤ I, ENETS stage ≥ IIb vs ENETS stage ≤ IIa).

Histologic Examination and Immunohistochemistry

Surgical specimens were fixed in 10% formalin and embedded in paraffin. Two pathologists (M.A. and M.K.), who were unaware of the clinical data, reviewed all the hematoxylin-and-eosin–stained sections and reclassified and graded the specimens according to the histologic parameters.

Serial 4-μm sections were used for immunohistochemical staining. Deparaffinized and rehydrated sections were immersed in 0.3% hydrogen peroxide in methanol for 30 minutes to block endogenous peroxidase activity. Heat-induced antigen retrieval was performed for 20 minutes at 95°C with a 10-mM citrate buffer (pH 6.0). After the slides had cooled at room temperature for 1 hour, they were exposed to 2% normal swine serum in phosphate-buffered saline for 30 minutes, then allowed to react overnight at 4°C with the following mouse monoclonal antibodies: antihuman geminin (diluted 1:40, clone EM6; Novocastra, Newcastle, United Kingdom) or antihuman Ki-67 (diluted 1:100, clone MIB-1; Dako, Glostrup, Denmark). After washing with phosphate-buffered saline 3 times, the sections were reacted with EnVision plus (Dako) for 30 minutes at room temperature. The peroxidase reaction products were developed with 3,3′-diaminobenzidine, and the sections were counterstained with hematoxylin.

The LI of each marker was calculated by manually counting the number of brown-stained tumor cell nuclei among the total number of tumor cells in the most highly immunoreactive area at a magnification of 400-fold, with the aid of an eyepiece grid (5 × 5 squares). Indices were expressed as a percentage value corresponding to the number of positive cells among approximately 2000 tumor cells.

Evaluation of Color Difference Quotation

Immunohistochemically stained full-face sections from each case with geminin and Ki-67 overexpression were digitized using the Slide Path and the NanoZoomer Digital Pathology System (Hamamatsu, Welwyn Garden City, United Kingdom). Approximately 7 minutes was required to scan a slide at a resolution of 40×. Subsequently, 400-fold magnified images from highly immunoreactive areas were exported for analysis.

The image analysis was performed using Photoshop (version 7; Adobe Systems, San Jose, CA). First, the image mode was converted from RGB to Lab color mode. Two hundred fifty representative positive cells were selected in each of 4 cases with high geminin expression levels (LI ≥ 2.0%) and 7 cases with high Ki-67 expression levels (LI ≥ 2.0%). All the cells with a recognizable brown stain were measured. The L*a*b* value of the nuclear areas was outputted as a range from 0 to 255. The values represented a Lab color space composed of 3 axes in a spherical form: L^*, a^*, and b^*. The L^* axis was associated with the lightness of the color, whereas the a^* and b^* axes were associated with the red-green scale and the yellow-blue scale, respectively. After the conversion of the scale to the CIE LAB color system, the L^* value was described as a decimal scale from 0 to 100, and the a^* and b^* values ranged from −128 to 127. The difference between the average values for a positive cell and an adjacent negative cell was calculated as ΔL^*, Δa^*, and Δb^*. Then, the color difference ΔE was estimated using the formula $\Delta E = [(\Delta L^*)^2 + (\Delta a^*)^2 + (\Delta b^*)^2]^{1/2}$. ΔE was then compared between the geminin-stained and Ki-67–stained sections.

Statistical Analysis

The Spearman rank correlation test was used to determine associations between continuous variables. Receiver operating characteristic curves were plotted to calculate the sensitivity, specificity, positive predictive value, and negative predictive value for the presence of metastasis. The cutoff values for the geminin LI and the Ki-67 LI were chosen so as to obtain the best combination of predictive values. A univariate analysis using the Cox proportional hazards model was applied to estimate the associations of clinicopathologic factors, including the immunohistochemical results, with the disease-free survival period. Survival curves were drawn using the Kaplan-Meier method, and the differences were analyzed using a log-rank test. Differences in nonparametric data were estimated using the Mann-Whitney U test. All P values < 0.05 were considered statistically significant. The statistical analyses were performed using Dr. SPSS II for Windows (SPSS Japan, Tokyo, Japan).

RESULTS

Demographic Characteristics and Tumor-Related Factors

Among the 27 patients, the median age at the time of diagnosis was 56 years; 14 patients (51.9%) were men, and 13 patients (48.1%) were women. In all the patients, a curative resection was performed, followed by a histologic assessment of the tumor grading. The tumor-related factors are summarized in Table 1. The tumor was located in the pancreatic head in 11 cases (40.7%), in the body in 12 cases (44.4%), and in the tail in 4 cases (14.8%). Only 1 case of functional PNET (insulinoma) was included. The median and range of the maximum tumor diameter were 26 mm and 8 to 92 mm, respectively. The diameter was 2 cm or larger in 11 cases (40.7%). Local invasion was observed in 2 cases (7.4%). One of these cases exhibited an obstruction of the inferior common bile duct, and another case presented with invasion to both the splenic artery and vein. Lymph node metastasis was encountered in 10 cases (37.0%), and a solitary liver metastasis was resected in 1 case (3.7%). With respect to mitosis, fewer than 2 mitoses per 10 HPFs were present in 19 cases (70.4%), from 2 to 10 mitoses per 10 HPFs were encountered in 8 cases (29.6%), and none of the cases had more than 20 mitoses per 10 HPFs.

The tumor grade classifications according to the WHO system and tumor staging according to the AJCC or ENETS criteria are shown in Table 1. Nineteen cases (70.4%) were classified as grade 1 neuroendocrine tumor (NET), and 8 cases

TABLE 1. Patient Demographics and Tumor-Related Factors for 27 Patients

Characteristics		
Age, y	Median	56
	Range	31–76
Sex, n (%)	Men	14 (51.9)
	Women	13 (48.1)
Location, n (%)	Ph	11 (40.7)
	Pb	12 (44.4)
	Pt	4 (14.8)
Functional tumor, n (%)		1 (3.7)
Maximum diameter, mm	Median	26
	Range	8–92
Diameter, n (%)	<2 cm	16 (59.3)
	≥2 cm	11 (40.7)
Local invasion, n (%)		2 (7.4)
Metastasis, n (%)	—	17 (63.0)
	Lymph node	10 (37.0)
	Liver	1 (3.7)
Mitosis, n (%)	0–1 per 10 HPFs	19 (70.4)
	2–20 per 10 HPFs	8 (29.6)
	>20 per 10 HPFs	0 (0.0)
WHO grading, n (%)	NET G1	19 (70.4)
	NET G2	8 (29.6)
	NEC	0 (0.0)
AJCC stage, n (%)	IA	8 (29.7)
	IB	9 (33.3)
	IIA	0 (0.0)
	IIB	9 (33.3)
	III	0 (0.0)
	IV	1 (3.7)
ENETS stage, n (%)	I	8 (29.7)
	IIa	7 (25.9)
	IIb	2 (7.4)
	IIIa	0 (0.0)
	IIIb	9 (33.3)
	IV	1 (3.7)

NET G1 indicates grade 1 NET; NET G2, grade 2 NET; Pb, pancreatic body; Ph, pancreatic head; Pt, pancreatic tail.

(29.6%) were classified as grade 2. According to the AJCC staging, 17 cases (63.0%), 9 cases (33.3%), 0 cases (0%), and 1 case (3.7%) were classified as stages I, II, III, and IV, respectively. According to the classification proposed by ENETS, 8 cases (29.7%), 9 cases (33.3%), 9 cases (33.3%), and 1 case (3.7%) were classified as stages I, II, III, and IV, respectively.

The median and range of the observation period were 1704 days and 37 to 4206 days, respectively. Three patients died, one of whom had a tumor-related death; the other 2 patients had treatment-related deaths. Recurrence after surgery was observed in 6 patients (22.2%).

Geminin and Ki-67 Expression

The immunohistochemical analysis examined the expressions of geminin and Ki-67 protein in all the cases (Fig. 1). Immunoreactivity was observed exclusively in the nuclei of the tumor cells. Geminin was also immunoreactive in the perichromosomal cytoplasm of mitotic cells in a few cases. The median LIs for geminin and Ki-67 were 1.0% and 1.5%, respectively. The geminin LI was slightly but significantly lower than that of Ki-67. Figure 2 shows the positive correlation between the geminin LI and the Ki-67 LI (Spearman $R_s = 0.757$, $P < 0.001$).

The receiver operating characteristic curves for the geminin LI, the Ki-67 LI, and the mitosis count (all of which were continuous variables), which were used to predict the presence of metastatic lesions, are shown in Figure 3. The curves for the 2 LIs were similar. The area under the curve was calculated to be 0.829 (95% confidence interval [CI], 0.660–0.999) for the geminin LI, 0.776 (95% CI, 0.598–0.955) for the Ki-67 LI, and 0.594 (95% CI, 0.362–0.826) for the mitosis count. The geminin LI seemed to have a slightly superior ability to predict metastasis, compared with the Ki-67 LI. The sensitivity, specificity, positive predictive value, and negative predictive value of a geminin LI greater than 2.0% (n = 4) and of a Ki-67 LI greater than 2.0% (n = 7) for determining metastasis were 33.3%, 90.5%, 50.0%, and 82.6% and 50.0%, 80.0%, 42.9%, and 85.0%, respectively. We defined high-geminin expression cases as those with a geminin LI greater than 2% because this cutoff had the best discriminatory power for the predictive values. According to the current WHO classification, a Ki-67 LI of 2.0% can be used to discriminate G1 tumors, and this cutoff also had the best discriminatory power for the predictive values in the present analysis. Thus, we regarded a Ki-67 LI greater than 2.0% as indicating a high Ki-67 expression level.

Correlations of Geminin and Ki-67 LIs With Prognosis

Because there was only 1 tumor-related death in this series, we examined the predictive values of each LI for the disease-free survival period after surgery. The results of a univariate Cox regression analysis are shown in Table 2. A mitosis count of 2 or more per 10 HPFs (hazard ratio [HR], 10.204; 95% CI, 1.684–61.834; $P = 0.012$), a local invasion (HR, 18.762; 95%

FIGURE 1. Representative photomicrograph of a PNET specimen. Hematoxylin and eosin staining (A) shows a typical trabecular arrangement of uniform tumor cells. The cells have eosinophilic cytoplasm and centrally located, round nuclei. Immunohistochemical staining for geminin (B) and Ki-67 (C) shows brown-stained tumor cell nuclei. The number of geminin-positive cells was smaller than the number of Ki-67–positive cells in most cases (original magnification ×400).

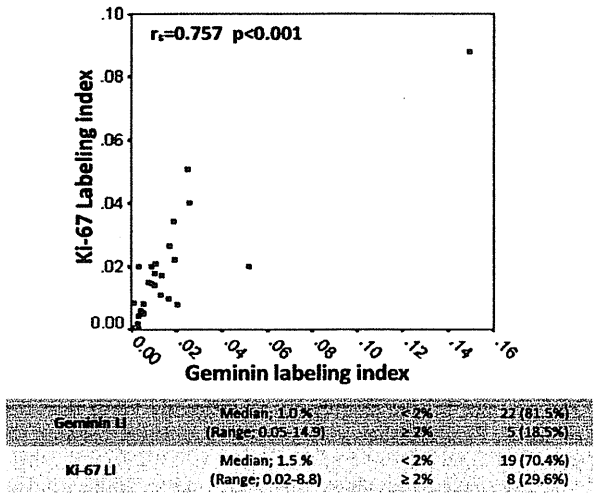

FIGURE 2. Scatterplot of the geminin LI and the Ki-67 LI (top) shows a positive correlation between the 2 LIs (Spearman rank correlation coefficient; $r_s = 0.757$; $P < 0.001$). The geminin expression level was lower than the Ki-67 expression level (bottom).

CI, 1.163–302.6; $P = 0.039$), a metastasis (HR, 10.469; 95% CI, 1.103–102.77; $P = 0.041$), a Ki-67 LI greater than 2.0% (HR, 6.182; 95% CI, 1.221–31.298; $P = 0.028$), a geminin LI greater than 2.0% (HR, 13.709; 95% CI, 1.919–97.739; $P = 0.009$), an AJCC stage of IIA or greater (HR, 8.758; 95% CI, 1.483–51.716; $P = 0.017$), and an ENETS stage of IIb or greater (HR, 16.793; 95% CI, 1.834–153.738; $P = 0.013$) were significantly correlated with recurrence. A multivariate Cox regression analysis revealed that none of these factors were independent prognostic factors. The Kaplan-Meier curves consistently exhibited a more significant relationship with the disease-free survival period after surgery for geminin (log rank, $P < 0.001$) than for Ki-67 (log rank, $P = 0.012$) (Fig. 4).

Concordance of Positivity Between Geminin and Ki-67 Stains

The immunoreactions were quantified using the CIE LAB color system. The color difference quotation was used to evaluate the positivity of the 2 stains. The color difference, ΔE, and a geminin-stained image are shown in Figure 5. The ΔE values

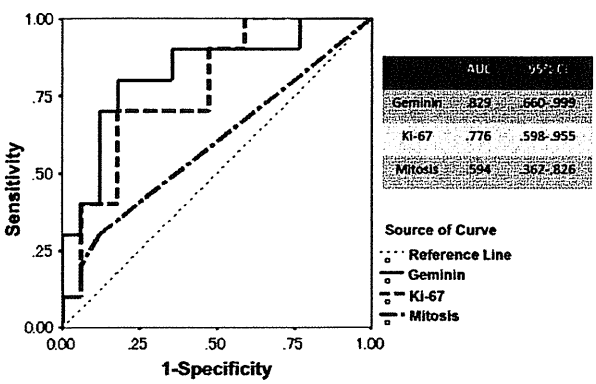

FIGURE 3. Receiver operating characteristic curves comparing the predictive value of the geminin LI to that of the Ki-67 LI or the mitosis count for determining the presence of metastasis.

TABLE 2. Univariate Cox Regression Analysis of Risk of Recurrence After Surgery

Variables	HR	95% CI	P
Diameter ≥2 cm	1.209	0.221–6.627	0.827
Mitosis ≥2 per 10 HPFs	10.204	1.684–61.834	0.012
v(+) or ly(+)	0.813	0.114–5.807	0.813
pn(+)	3.615	0.375–34.837	0.266
s(+) or rp(+)	2.068	0.411–10.4	0.378
Local invasion (+)	18.762	1.163–302.6	0.039
Metastasis (+)	10.469	1.103–102.77	0.041
Ki-67 LI >2.0%	6.182	1.221–31.298	0.028
Geminin LI >2.0%	13.709	1.919–97.739	0.009
WHO grade G2	2772.5	0.000–95.889 × 10^7	0.429
AJCC stage ≥IIA	8.758	1.483–51.716	0.017
ENETS stage ≥IIb	16.793	1.834–153.74	0.013

Local invasion indicates (+), presence of local invasion; ly(+), presence of lymphatic invasion; metastasis (+), presence of metastasis; pn(+), presence of peri-neural invasion; rp(+), presence of retroperitoneal invasion; s(+), presence of serosal invasion; v(+), presence of venous invasion.

corresponded with the optical intensity of the positive cells. The same consistency was observed for the images with Ki-67 staining (data was not shown). The distributions of ΔE in the geminin and Ki-67 staining images are shown in Figure 6. $\Delta E = 0$ signified no color difference from negative cells, and the left side of the histogram's distribution indicates the number of cells with equivocal positivity. A larger ΔE reflects a greater color disparity between the positive and negative cells. The medians (ranges) of the ΔE values for geminin and Ki-67 staining were

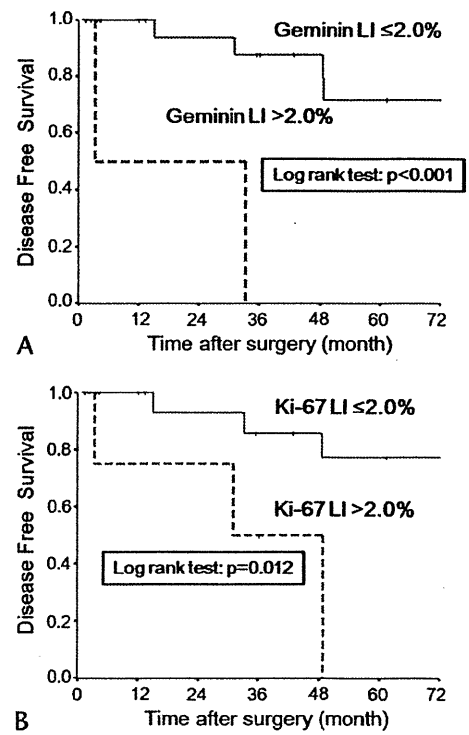

FIGURE 4. Disease-free survival period after surgery according to the geminin LI (A) and the Ki-67 LI (B).

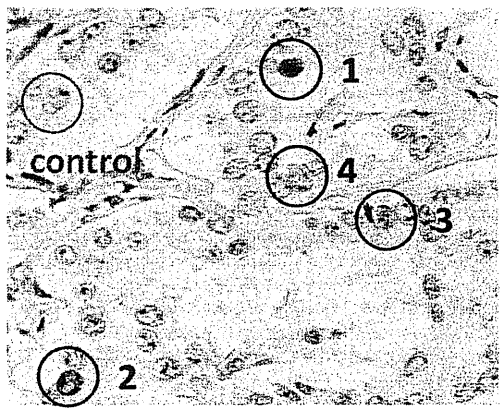

#	L* value	a* value	b* value	ΔE
1	65.17	-1.22	15.30	26.22
2	67.90	7.30	11.63	21.87
3	77.14	5.71	5.74	11.10
4	82.30	3.29	-0.71	2.51
Ctr	83.94	2.82	-2.55	

FIGURE 5. The color difference ΔE in geminin stain is shown. ΔE values were calculated from the difference of L*a*b* values between positive cells (in numbered red circles) and a negative cell (in green circle).

16.12 (5.8–41.8) and 13.17 (3.4–37.9), respectively. The ΔE for the geminin stain was significantly larger than that for the Ki-67 stain ($P < 0.001$).

DISCUSSION

The criteria used to predict the outcome of patients with PNET has been simplified in the 2010 WHO classification.[6] Pancreatic neuroendocrine tumors are divided into well-differentiated NETs and poorly differentiated neuroendocrine carcinoma (NEC). The definition of NEC is the presence of more than 20 mitoses per 10 HPFs. Neuroendocrine tumors were further subcategorized as low-grade NET (G1), characterized by the presence of 0 to 1 mitoses and a Ki-67 LI of 0% to 2%, and intermediate-grade NET (G2), characterized as 2 to 20 mitoses per 10 HPFs and a Ki-67 LI of 3% to 20%. Actually, immunohistochemical staining for Ki-67 has been the most reliable modality for assessing the proliferative activity.[2,3,7] In addition, staging has been noted to be an independent prognostic indicator, and the AJCC staging manual and the staging classification proposed by the ENETS are thought to be useful for predicting the prognosis of patients with PNET. In the present study, 19 and 8 cases were classified as G1 and G2, respectively. No cases of NEC were seen, consistent with the presence of only 1 tumor-related death. Regarding recurrence after radical resection, this grading system is not a reliable prognostic factor (Table 2). Unlike the WHO grading, however, both the AJCC and ENETS stagings are significantly correlated with recurrence; similarly, the superiority of these stagings to anticipate disease-free survival has been previously reported.[25] The present analysis suggested that local spread beyond the pancreas might be a key event.

The usefulness of geminin staining to predict the outcome of several neoplasms has been demonstrated using retrospective analyses.[17–22] The present study also indicated that geminin expression was a more useful indicator of disease-free survival than not only Ki-67 expression but also AJCC and ENETS staging (Table 2). Geminin expression is specifically limited during the S, G2, and early M phases, and it probably reflects the proliferative activity more precisely than these other factors. Indeed, the number of positive tumor cells for geminin was significantly smaller than that for Ki-67. Although the survival analysis using Kaplan-Meier curves suggested that the geminin LI was more associated with the prognosis than the Ki-67 LI (Fig. 4), the present study has a limitation to evaluate the prognosis in accordance with the small number of cases. Further analyses of a larger population is needed to determine the prognostic use of the geminin LI. Moreover, the mechanism by which geminin expression contributes to the aggressiveness of neoplasms remains unknown. The inhibition of Cdt1 by geminin has been regarded as a pivotal event in the licensing of DNA replication, so an increase in Cdt1 inhibition biologically results in cell cycle arrest. This discrepancy between geminin expression and cell proliferation remains to be explained. The predictive superiority of the geminin LI to the Ki-67 LI in the present analysis may depend on some aspect of the malignant potential other than the proliferative activity.

In addition, the immunoreactivity of geminin staining in each tumor cell was relatively clear, whereas weak positivity for Ki-67 staining was observed in some tumor cells (Fig. 1). Thus, fewer intraobserver and interobserver differences between pathologists or institutions can be expected using the geminin LI. Actually, the difficulty in grading PNETs has been attributed to the need for concordance, along with the lower frequencies of proliferative marker positivity in PNETs. In the present study, we performed a color difference quotation analysis using the CIE LAB color system. Several color analyses have reported that the

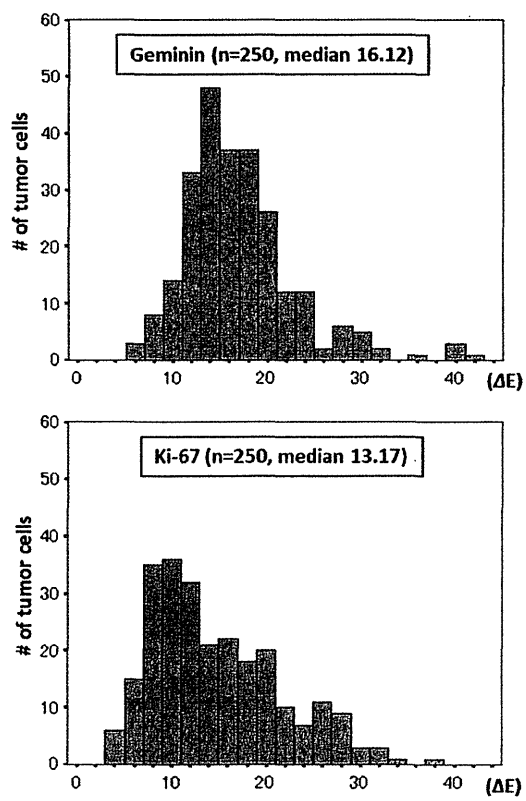

FIGURE 6. The distribution of each ΔE in geminin and Ki-67 stain is shown. The difference of each ΔE was evaluated as statistically significant ($P < 0.001$) using the Mann-Whitney U test.

color parameters of the CIE LAB color system are closely related to the psychophysical characteristics of color perception.[26–28] This analysis was the first application of the CIE LAB color system for the quantification of immunohistochemical positivity. As shown in Figure 5, a precise correspondence between ΔE and the optical color intensities was observed. Furthermore, the ΔE for geminin staining was larger than that for Ki-67 staining. These results suggest that a greater concordance was achieved using the geminin LI rather than the Ki-67 LI. The use of the color difference quotation enabled subjective optical intensities to be measured as absolute values, and no inconsistencies with regard to determining positivity were encountered. Thus, the CIE LAB color system may be a promising tool for making objective histopathologic assessments.

Pancreatic neuroendocrine tumor constitutes a heterogeneous group of rare neoplasms. Recent advances in abdominal imaging techniques have increased the detection of incidental nonfunctional PNET. In particular, endoscopic ultrasound and endoscopic ultrasound–guided fine needle aspiration biopsy procedures have drastically improved diagnostic accuracy.[29] Nowadays, minimally invasive surgery is usually recommended as a pancreas-preserving maneuver.[30] Therefore, accurate estimates of the malignant potential before surgery are becoming increasingly important for optimal patient management. Despite the importance of such estimations, pretreatment evaluations remain difficult. Only microscopic observations are acceptable for tumor grading and staging because PNET can exhibit heterogeneous biological behavior even within the same tumor. In the present study, a heterogeneous expression level was observed throughout the tumor for both geminin and Ki-67 staining. The use of geminin expression for the assessment of biopsy samples or aspirated specimens was not evaluated in the present study. Thus, the establishment of a preoperative classification based on geminin expression will require further research.

In conclusion, the geminin expression level in PNETs was correlated with the disease-free survival period after curative resection. The geminin LI may be more useful than the Ki-67 LI for predicting postoperative outcome.

ACKNOWLEDGMENT

The authors thank Dr Hiroshi Yamaguchi and Dr Toshio Ohmori, Imaging Technology Center, FUJIFILM Corp, Minamiashigara, Japan, for their technical advice.

REFERENCES

1. Imamura M. Recent standardization of treatment strategy for pancreatic neuroendocrine tumors. *World J Gastroenterol.* 2010;16(36):4519–4525.
2. Ferrone CR, Tang LH, Tomlinson J, et al. Determining prognosis in patients with pancreatic endocrine neoplasms: can the WHO classification system be simplified? *J Clin Oncol.* 2007;25(35):5609–5615.
3. Pelosi G, Bresaola E, Bogina G, et al. Endocrine tumors of the pancreas: Ki-67 immunoreactivity on paraffin sections is an independent predictor for malignancy: a comparative study with proliferating-cell nuclear antigen and progesterone receptor protein immunostaining, mitotic index, and other clinicopathologic variables. *Hum Pathol.* 1996;27(11):1124–1134.
4. Hochwald SN, Zee S, Conlon KC, et al. Prognostic factors in pancreatic endocrine neoplasms: an analysis of 136 cases with a proposal for low-grade and intermediate-grade groups. *J Clin Oncol.* 2002;20(11):2633–2642.
5. Phan GQ, Yeo CJ, Hruban RH, et al. Surgical experience with pancreatic and peripancreatic neuroendocrine tumors: review of 125 patients. *J Gastrointest Surg.* 1998;2(5):473–482.
6. Bosman FT, Carneiro F, Hruban RH, eds. *WHO Classification of Tumours of the Digestive System.* 4th ed. Lyon, France: IARC; 2010.
7. Ekeblad S, Skogseid B, Dunder K, et al. Prognostic factors and survival in 324 patients with pancreatic endocrine tumor treated at a single institution. *Clin Cancer Res.* 2008;14(23):7798–7803.
8. La Rosa S, Sessa F, Capella C, et al. Prognostic criteria in nonfunctioning pancreatic endocrine tumours. *Virchows Arch.* 1996;429(6):323–333.
9. Gentil Perret A, Mosnier JF, Buono JP, et al. The relationship between MIB-1 proliferation index and outcome in pancreatic neuroendocrine tumors. *Am J Clin Pathol.* 1998;109(3):286–293.
10. Clarke MR, Baker EE, Weyant RJ, et al. Proliferative activity in pancreatic endocrine tumors: association with function, metastases, and survival. *Endocr Pathol.* 1997;8(3):181–187.
11. Gerdes J, Lemke H, Baisch H, et al. Cell cycle analysis of a cell proliferation–associated human nuclear antigen defined by the monoclonal antibody Ki-67. *J Immunol.* 1984;133(4):1710–1715.
12. Scholzen T, Gerdes J. The Ki-67 protein: from the known and the unknown. *J Cell Physiol.* 2000;182(3):311–322.
13. Wohlschlegel JA, Kutok JL, Weng AP, et al. Expression of geminin as a marker of cell proliferation in normal tissues and malignancies. *Am J Pathol.* 2002;161(1):267–273.
14. Takeda DY, Dutta A. DNA replication and progression through S phase. *Oncogene.* 2005;24(17):2827–2843.
15. McGarry TJ, Kirschner MW. Geminin, an inhibitor of DNA replication, is degraded during mitosis. *Cell.* 1998;93(6):1043–1053.
16. Wohlschlegel JA, Dwyer BT, Dhar SK, et al. Inhibition of eukaryotic DNA replication by geminin binding to Cdt1. *Science.* 2000;290(5500):2309–2312.
17. Gonzalez MA, Tachibana KE, Chin SF, et al. Geminin predicts adverse clinical outcome in breast cancer by reflecting cell-cycle progression. *J Pathol.* 2004;204(2):121–130.
18. Dudderidge TJ, Stoeber K, Loddo M, et al. Mcm2, geminin, and KI67 define proliferative state and are prognostic markers in renal cell carcinoma. *Clin Cancer Res.* 2005;11(7):2510–2517.
19. Dudderidge TJ, McCracken SR, Loddo M, et al. Mitogenic growth signalling, DNA replication licensing, and survival are linked in prostate cancer. *Br J Cancer.* 2007;96(9):1384–1393.
20. Yamazaki M, Fujii S, Murata Y, et al. High expression level of geminin predicts a poor clinical outcome in salivary gland carcinomas. *Histopathology.* 2010;56(7):883–892.
21. Haruki T, Shomori K, Hamamoto Y, et al. Geminin expression in small lung adenocarcinomas: implication of prognostic significance. *Lung Cancer.* 2011;71(3):356–362.
22. Shomori K, Nishihara K, Tamura T, et al. Geminin, Ki67, and minichromosome maintenance 2 in gastric hyperplastic polyps, adenomas, and intestinal-type carcinomas: pathobiological significance. *Gastric Cancer.* 2010;13(3):177–185.
23. Edge SB, Byrd DR, Compton CC, et al, eds. *AJCC Cancer Staging Manual.* 7th ed. New York, NY: Springer; 2010.
24. Rindi G, Kloppel G, Alhman H, et al. TNM staging of foregut (neuro)endocrine tumors: a consensus proposal including a grading system. *Virchows Arch.* 2006;449(4):395–401.
25. La Rosa S, Klersy C, Uccella S, et al. Improved histologic and clinicopathologic criteria for prognostic evaluation of pancreatic endocrine tumors. *Hum Pathol.* 2009;40(1):30–40.
26. Jorn D, Waddell JN, Swain MV. The influence of opaque application methods on the bond strength and final shade of PFM restorations. *J Dent.* 2010;38(suppl 2):e143–e149.
27. Kim JY, Kim JW, Seo SH, et al. A novel consistent photomicrography technique using a reference slide made of neutral density filter. *Microsc Res Tech.* 2011;74(5):397–400.
28. Kinnunen J, Jurvelin JS, Makitalo J, et al. Optical spectral imaging of degeneration of articular cartilage. *J Biomed Opt.* 2010;15(4):046024.
29. Figueiredo FA, Giovannini M, Monges G, et al. Pancreatic endocrine tumors: a large single-center experience. *Pancreas.* 2009;38(8):936–940.
30. Casadei R, Ricci C, Rega D, et al. Pancreatic endocrine tumors less than 4 cm in diameter: resect or enucleate? A single-center experience. *Pancreas.* 2010;39(6):825–828.

J Hepatobiliary Pancreat Sci (2012) 19:249–258
DOI 10.1007/s00534-011-0416-3

ORIGINAL ARTICLE

Compliance with and effects of preoperative immunonutrition in patients undergoing pancreaticoduodenectomy

Hirofumi Shirakawa · Taira Kinoshita · Naoto Gotohda · Shinichiro Takahashi · Toshio Nakagohri · Masaru Konishi

Published online: 11 June 2011

Abstract
Background/purpose This study was conducted to ascertain the feasibility and effectiveness of preoperative enteral immunonutrition using an immune-enhanced formula (Impact) in patients undergoing pancreaticoduodenectomy.
Methods Twenty-five patients undergoing an elective pancreaticoduodenectomy were asked to ingest Impact for 5 days (750 mL/day) prior to surgery in addition to their normal diets. We retrospectively compared the early postoperative outcomes of the Impact group ($n = 18$), which consisted of patients who fully complied with the study protocol, and a control group ($n = 13$), which consisted of patients who had not ingested Impact prior to surgery.
Results Overall, 82.6% of the patients complied with the preoperative oral ingestion of Impact; all but four patients tolerated a daily intake of 750 mL. While the clinical backgrounds of the Impact and control groups were not significantly different, the frequency of incisional wound infection was lower (0 vs. 30.8%, $p = 0.012$) and the change in systemic severity as evaluated using the acute physiology and chronic health evaluation (APACHE)-II scoring system was milder ($p = 0.033$) in the Impact group than in the control group.
Conclusion The preoperative oral ingestion of Impact was well tolerated and appeared to be effective for preventing incisional wound infection and reducing the response to surgical stress in patients undergoing a pancreaticoduodenectomy.

Keywords Immunonutrition · Pancreaticoduodenectomy · Surgical site infection · Nutrition

H. Shirakawa · T. Kinoshita · N. Gotohda · S. Takahashi · T. Nakagohri · M. Konishi
Hepatobiliary Pancreatic Surgery Division,
National Cancer Center Hospital East,
6-5-1 Kashiwanoha, Kashiwa 277-8577, Chiba, Japan

H. Shirakawa (✉)
Department of Surgery, Tochigi Cancer Center,
4-9-13 Yohnan, Utsunomiya 320-0834, Tochigi, Japan
e-mail: hshiraka@tcc.pref.tochigi.lg.jp

Introduction

In recent years, pancreaticoduodenectomy (PD) has gained acceptance as an appropriate surgical procedure for selected patients with diseases of the pancreas head and periampullary region. Improvements in surgical techniques and accumulating experience have reduced the complication rate after PD. The postoperative mortality rates after PD are typically 5% or less at major surgical centers [1, 2], although the morbidity rates remain high, ranging from 10 to 50% [3–5]. Thus, postoperative morbidity after PD remains problematic and can lead to delays in the postoperative resumption of adequate oral food intake. Even in series with relatively good rates of postoperative morbidity, about 10% of the patients develop wound infections [1, 3–6]. However, the morbidity rate increases considerably if other complications, such as pancreatic fistula or delayed gastric emptying, are included [7]. Bacteria from the gut, especially Enterococci and *Escherichia coli* [8], translocate into the mesenteric lymph nodes or blood, where they cause the majority of the observed infections. Several conditions before, during, or after surgery can facilitate this bacterial translocation, including a reduction in postoperative intestinal motility, jaundice, the use of antibiotics resulting in small bowel bacterial overgrowth [9], the loss

of mucosal barrier function caused by malnutrition, manipulation of the bowel, and parenteral nutrition [10].

Recently, enteral immune-enhancing formulas supplemented with arginine, omega-3 fatty acids, and ribonucleic acid (RNA) have been suggested to improve the immune response and wound healing in postoperative patients [11, 12]. Arginine, which is classified as a semi-essential amino acid for catabolism, serves as a substrate for the urea cycle and the production of nitric oxide during protein synthesis. Arginine is known to promote T cells and to have a direct enhancing effect on their activities [13], enhancing the phagocytosis of neutrophils. Arginine also reduces the production of inflammatory mediators, such as interleukin (IL)-1beta, tumor necrosis factor alpha (TNF-α), and IL-6 at the site of tissue injury and is capable of enhancing cellular immunity in rat septic models [14]. Finally, arginine accelerates tissue growth after infection [15]. Omega-3 fatty acids compete with omega-6 fatty acids for cyclo-oxygenase metabolism at the cell membrane and for the production of eicosapentanoic acid (EPA). In addition, omega-3 fatty acids increase the production of some prostaglandins (PGs) and leukotrienes, reducing the proinflammatory potential, and inhibit the production of some other PGs (PGE2) and leukotrienes, reducing the cytotoxicity of macrophages, lymphocytes, and natural killer (NK) cells [11]. Supplementation with agents rich in omega-3 fatty acids also decreases prostacyclin and thromboxane (TX)-A2 synthesis and increases the antiaggregatory substance TXA3 [16]. Omega-3 fatty acids and EPA are believed to inhibit excessive inflammatory responses but not to be immunosuppressive. The intravenous administration of omega-3 fatty acids significantly reduced the production of proinflammatory cytokines in a recent clinical trial in patients with sepsis [17]. RNA supplementation is necessary for the proliferation of immune cells or cells involved in wound healing [18].

Several studies have demonstrated that immune-enhancing formulas may improve the postoperative immune response and reduce inflammatory reactions in various groups of postoperative patients, thereby reducing the incidence of serious infectious complications [12, 19–25]. Thus, the preoperative administration of these formulas in patients undergoing gastrointestinal tract surgery has been recommended [15, 24, 26–29]. In Japan, an enteral diet was introduced for immunonutrition in 2002; however, to the best of our knowledge, the utility of preoperative immunonutrition in patients undergoing PD has yet to be examined. The present study was undertaken to determine whether the preoperative oral intake of an immune-enhancing formula may be suitable for patients undergoing elective PD. Furthermore, we attempted to evaluate the effect of a preoperative immune-enhancing formula containing arginine, omega-3 fatty acids, and RNA (Impact Japanese version; Ajinomoto, Tokyo, Japan) on the early postoperative outcomes of patients, comparing outcomes with a historical control group who had received a normal diet alone.

Patients, materials, and methods

From February 2005 to November 2006, 25 consecutive patients (19 men, 6 women; age range, 48–77 years; median age, 64 years) who were candidates for a curative PD for the resection of a lesion in either the pancreatic head or the periampullary region were prospectively enrolled. The study protocol was reviewed and approved by the institutional review board of our hospital. Consenting patients who did not have malnutrition, bowel obstruction, severe cardiopulmonary complications, diabetes, collagen disease, renal failure, ongoing infection, or immune disorders were enrolled in the study. None of the patients had an immunosuppressive condition preoperatively. Patients were required to sign a written informed consent form once the protocol was explained.

The subjects included 5 patients with pancreatic invasive ductal carcinoma (PIDC), 6 with intraductal papillary mucinous neoplasm (IPMN), 9 with biliary tract cancers [bile duct cancer (BDC) in 6 and carcinoma of the papilla of Vater (VC) in 3], 3 with duodenal carcinoma, and 2 with other diseases (a pancreatic solid and pseudo-papillary neoplasm in 1 and a serous cystic adenoma in 1).

First, patient compliance with the preoperative ingestion of Impact was examined. After hospitalization, the patients were instructed to consume 3 packs/day (750 mL) of Impact Japanese version (Ajinomoto) in addition to their normal diets over a 5-day period immediately before surgery. Regarding the timing of the enteral immunonutrition, studies examining gastrointestinal cancer patients without malnutrition have reported that because a sufficient effect could be achieved with 5 days of preoperative administration, the postoperative administration of Impact was not necessary [26, 30]. In the study by Braga et al. [26], 1000 mL/day of Impact was prescribed to patients without malnutrition, but the actual mean intake was 890 mL. Because the mean body size of Japanese is smaller than that of Westerners, the daily intake of Impact Japanese version was set at 3 packs/day (750 mL/day) in the present study. Impact Japanese version is based on Impact (Novartis Consumer Health, Bern, Switzerland), and has been designed to suit the nutritional needs and flavor preferences of Japanese populations. A total of 750 mL of Impact Japanese version contains 9.6 g of arginine, 2.49 g of omega-3 fatty acids, and 0.96 g of RNA. The kilocalorie/milliliter ratio is 1:1. Regular meals of 1800 or 2000 kcal/day, depending on the patient's body size, were served preoperatively.

The patients were admitted at least 1 week before surgery and underwent mechanical preparation, including the oral intake of 2 L of polyethylene glycol electorolyte lavage solution (Niflec; Ajinomoto). Preoperative cultures were performed using nasal and throat swabs from all the patients to test for methicillin-resistant *Staphylococcus aureus* (MRSA). As a preventative antibiotic, 1 g of cefmetazole sodium (CMZ) (Cefmetazone; Daiichi Sankyo, Tokyo, Japan) was administered intravenously via a drip infusion immediately after the induction of anesthesia. A second dose was given 3 h later, followed by doses every 12 h for 2 days after the surgery. Oral feeding was initiated 5 days after the surgery.

Second, we attempted to evaluate the early postoperative outcome after PD by comparing the Impact group, which consisted of patients who fully complied with the ingestion of Impact for 5 days preoperatively, with a control group, which consisted of patients with a similar clinical background and condition who had undergone the same operative procedure in our hospital in 2004 but who had not ingested an immune-enhanced formula preoperatively. The age, sex, body mass index (BMI), serum albumin level, prognostic nutrition index (PNI) [31], preoperative biliary drainage, operative methods, operation times, and intraoperative blood loss of the two groups were compared. Regarding the postoperative course, the surgical morbidity and mortality and the duration of the hospital stay were investigated. The presence of postoperative complications, such as pancreatic fistula and incisional wound infection, and the infection status were described in the medical records. Incisional wound infection was defined based on the evidence of purulent exudate in the wound and the isolation of pathogenic organisms in culture. Surgical site infection (SSI) was diagnosed according to the Centers for Disease Control (CDC) definitions of SSI [32].

During the perioperative period, laboratory blood tests were performed. The white blood cell (WBC) count and the C-reactive protein (CRP), total protein (TP), serum albumin (Alb), total bilirubin (T-Bil), serum amylase (AMY), glutamic oxaloacetic transaminase (GOT), glutamic pyruvic transaminase (GPT), blood urea nitrogen (BUN), and serum creatinine (Cr) levels were routinely measured at 1, 3, and 7 days after surgery. Changes in body weight (BW), and in the acute physiology and chronic health evaluation (APACHE)II scores [33], and the duration of systemic inflammatory response syndrome (SIRS) in the postoperative course were also investigated. The APACHE-II classification includes twelve physiological measures (temperature, mean arterial pressure, heart rate, respiratory rate, oxygenation, arterial pH, serum sodium, serum potassium, serum creatinine, hematocrit, WBC count, and Glasgow Coma Scale score), age, and the presence of severe chronic health problems. The worst value in each patient was used as the physiological score. This index enables the prediction of perioperative events in patients undergoing various surgical procedures [34–39]. The definition of SIRS was adopted from the report by the American College of Chest Physicians/Society of Critical Care Medicine Consensus Conference [40]. SIRS was defined as the presentation of two or more of the following criteria: (1) temperature >38°C or <36°C; (2) heart rate >90 beats/min; (3) respiration >20/min or $PaCO_2$ <32 mmHg; (4) leukocyte count >12,000/mm^3, <4000/mm^3, or >10% band cells.

Statistical analysis of the data was performed using an unpaired Student's *t*-test, the χ^2 test, and the Mann–Whitney *U*-test. Variations in some parameters over time and comparisons among the two groups were studied using a repeated measure analysis of variance (ANOVA). Data are shown as means (standard deviation). All statistical analyses were performed using StatView-J 5.0 (Abacus Concepts, Berkeley, CA, USA); all two-sided p values <0.05 were considered statistically significant.

Operation procedures

Five staff surgeons performed all the operations. The operative procedure was a standardized substomach-preserving PD. Reconstruction was achieved using a retrocolic jejunal Roux-en-Y limb with an end-to-side pancreaticojejunostomy, an end-to-side hepaticojejunostomy, and a gastrojejunostomy, according to the child procedure. In all patients, a pancreatic stenting tube was placed in the pancreatic duct and fixed with 2 absorbable suture ligations. The main duct was anchored to the adjacent serosa. A 3-0 polypropylene monofilament thread with curved needle was prepared with a straightened needle at each end. The suture was passed from the ventral to the dorsal surface of the pancreas from the cut end and the serosal surface of the jejunum. All end-to-side pancreaticojejunostomies were performed in two layers. The inner layer comprised the opposition of the pancreatic duct and adjacent pancreatic tissue to a small opening in the jejunum (full thickness), which was made by puncturing the tissues with a thick needle connected to the pancreatic stenting tube and utilizing interrupted stitches of 5-0 monofilament polyglyconate. All pancreaticojejunal anastomoses were stented (decompressed) through 6- or 7.5-F polyvinyl chloride tubes, according to the diameter of the main pancreatic duct, and the tubes were guided externally through the jejunal loop. The pancreatic juice was completely drained via the tube, and the tube was removed 3 weeks or more after the surgery.

Hepaticojejunostomy was performed using interrupted polyglyconate sutures. A stenting tube was not inserted through the anastomosis in any of the patients. Penrose drains were routinely placed on the anterior and posterior

Table 1 List of patients with preoperative Impact consumption

Patient	Age (years)	Sex	Disease	Procedure	Duration of oral intake of Impact (days)	Reasons for discontinuation of Impact
1	79	Female	BDC	SSpPD	5	None
2	57	Female	PIDC	SSpPD	5	None
3	58	Male	IPMN	SSpPD	5	None
4	68	Male	VC	SSpPD	5	None
5	77	Male	BDC	SSpPD	5	None
6	68	Male	DC	SSpPD	1	Diarrhea
7	52	Male	BDC	SSpPD	5	None
8	56	Male	IPMN	SSpPD	5	None
9	62	Female	IPMN	SSpPD	5	None
10	77	Male	VC	SSpPD	2	Nausea
11	57	Male	BDC	EBDR	5	None
12	75	Male	BDC	Not resected	3	Diarrhea
13	64	Female	PIDC	SSpPD	5	None
14	48	Male	IPMN	SSpPD	4	Pancreatitis and cholangitis
15	62	Male	IPMN	SSpPD	5	None
16	57	Female	VC	SSpPD	5	None
17	67	Male	DC	SSpPD	5	None
18	59	Male	SPT	SSpPD	5	None
19	64	Male	PIDC	SSpPD	5	None
20	62	Female	DC	SSpPD	5	None
21	72	Male	BDC	SSpPD	5	None
22	67	Male	PIDC	SSpPD	5	None
23	44	Female	SCT	SSpPD	5	None
24	58	Male	IPMN	SSpPD	3	Changed operation date
25	64	Male	PIDC	Not resected (GJB)	1	Changed operation date

BDC bile duct carcinoma, *PIDC* pancreatic invasive ductal carcinoma, *IPMN* intraductal papillary mucinous neoplasm, *VC* papilla of Vater carcinoma, *DC* duodenal carcinoma, *SPT* solid and pseudo-papillary tumor of pancreas, *SCT* serous cystic tumor of pancreas, *SSpPD* substomach-preserving pancreaticoduodenectomy, *EBDR* extra bile duct resection, *GJB* gastrojejunal bypass

surfaces of the pancreaticojejunal anastomosis and the dorsal side of the hepaticojejunostomy.

Reconstruction was completed before suturing the abdominal wall. Immediately after the opening of the abdomen, the surgical wound was protected by the placement of a drape. Before closing the abdomen, the abdominal cavity was washed using 3000 mL of warm saline, and the drape was removed. The surgeon and assistant changed gloves, and the abdominal muscle and fascia layers were closed using monofilament absorbable sutures. After washing the skin and subcutaneous fat layer with 500 mL of warm saline, the wound was closed using a skin stapler. Postoperatively, the wound was covered using a transparent protective film and was monitored without sterilization until suture removal.

Results

Compliance with preoperative administration of Impact

The amount of the immunonutrition preparation consumed preoperatively was monitored by the doctor in charge of each patient. A total of 25 patients were enrolled in the study (see Table 1). As the scheduled operation date was moved forward for two patients, these 2 patients had to discontinue Impact consumption. Treatment compliance and other reasons for discontinuation are summarized in Table 2. Nineteen patients (82.6%) fully complied with Impact consumption. The mean period of preoperative oral intake was 4.6 ± 1.1 days. The reasons for the discontinuation of Impact consumption were diarrhea in 2 patients, nausea in 1 patient, and pancreatitis and cholangitis caused by the primary disease in 1 patient. The nausea and diarrhea symptoms occurred 3 days after the start of Impact consumption.

Comparison of early postoperative outcome after PD between the Impact and control groups

Of the 25 patients, 18 were able to complete the Impact consumption protocol. These patients (Impact group) were retrospectively compared with a control group consisting of patients treated at our institution in 2004 who had undergone the same surgical procedure for the treatment of

similar conditions but who had not ingested an immune-enhanced formula preoperatively.

The preoperative and intraoperative clinical background characteristics of the two groups of patients are summarized in Table 3. No significant difference was observed in the total numbers of calories served in the daily hospital meals given for 5 days before surgery and until postoperative day (POD) 7 between the two groups (data not shown). In both the Impact and control groups, peripheral parenteral nutritional infusion was used, without using total parenteral nutrition. Moreover, no differences in age, sex, preoperative nutritional status, operative time, or intraoperative blood loss were observed between the groups.

Table 2 Compliance with oral intake of Impact

Duration of oral intake of immunonutrition (days)	4.6 ± 1.1
No. of patients who completed oral intake	19/23[a] (82.6%)
No. of patients who discontinued treatment	4/23[a] (17.4%)
Reasons for discontinuation	
Diarrhea	2 (8.7%)
Nausea	1 (4.3%)
Pancreatitis and cholangitis caused by primary disease	1 (4.3%)

[a] Not including 2 patients (out of a total of 25 patients in this study) who discontinued preoperative Impact consumption because of changed operation dates

Postoperative SIRS duration and complications

The duration and complications associated with postoperative SIRS in each group are shown in Table 4. The duration of postoperative SIRS and the hospital stay were not significantly different between the groups. The incidences of individual complications were also comparable between the groups. The incidence of incisional wound infection was significantly lower in the Impact group than in the control group (0 vs. 30.8%; $p = 0.012$), but no significant differences in the incidences of other postoperative complications were seen between the groups. The operative mortality rate was 0% for each group.

The effects of immune-enhanced nutrition on laboratory and physical data (WBC count, CRP level, TP, Alb, T-Bil, AMY, GOT, GPT, BUN, Cr, BW, and APACHE-II score) during the perioperative period are shown in Fig. 1. No significant differences in the WBC counts, CRP levels, TP, Alb, T-Bil, AMY, GOT, BUN, and Cr results were seen between the two groups. However, the GPT level was significantly higher in the Impact group (Fig. 1h). While the change in BW during the perioperative period also did

Table 3 Baseline patient characteristics

	Impact ($n = 18$)	Control ($n = 13$)	p
Age (years)	62.6 ± 8.5	65.1 ± 10.0	0.466
Sex (male/female)	11/7	7/6	0.686
BMI	21.9 ± 2.1	22.1 ± 3.2	0.821
Serum albumin (g/dL)	3.9 ± 0.3	3.7 ± 0.5	0.296
PNI	46.5 ± 5.8	43.7 ± 5.0	0.176
Biliary drainage	7	8	0.213
PTBD	5 (71.4%)	5 (62.5%)	0.714
ENBD	2 (28.6%)	3 (27.5%)	
Duration of oral intake of Impact (days)	5	None	None
Resection procedure	SSpPD		
Reconstruction method	Modified child method		
Operation time (min)	329 ± 79	308 ± 88	0.488
Intraoperative blood loss (mL)	921 ± 566	947 ± 654	0.905
Pathological diagnosis			
PIDC	4 (22.2%)	2 (15.4%)	
IPMN			
IPMA	3 (16.7%)	1 (7.7%)	
IPMC	0	1 (7.7%)	
SPT	1 (5.6%)	0	
SCA	1 (5.6%)	0	
BDC	5 (27.8%)	3 (23.1%)	
VC	2 (11.1%)	4 (30.8%)	
DC	2 (11.1%)	2 (15.4%)	

BMI body mass index, *PNI* prognostic nutrition index = (10 × serum albumin) + [0.005 × total lymphocyte count (/mm^3)], *PTBD* percutaneous transhepatic biliary drainage, *ENBD* endoscopic naso-biliary drainage, *SSpPD* substomach-preserving pancreaticoduodenectomy, *PIDC* pancreatic invasive ductal carcinoma, *IPMN* intraductal papillary mucinous neoplasm, *IPMA* intraductal papillary mucinous adenoma, *IPMC* intraductal papillary mucinous carcinoma, *SPT* solid and pseudo-papillary tumor, *SCT* serous cystic adenoma, *BDC* bile duct carcinoma, *VC* papilla of Vater carcinoma, *DC* duodenal carcinoma

Table 4 Early postoperative outcome and complications

	Impact (n = 18)	Control (n = 13)	p
Duration of postoperative SIRS (days)	0.8 ± 1.0	0.9 ± 0.8	0.664
Duration of postoperative hospital stay (days)	29 ± 13	26 ± 12	0.516
Morbidity and mortality			
Pancreatic fistula	12 (66.7%)	8 (61.5%)	0.768
Delayed gastric emptying	2 (11.1%)	1 (5.9%)	0.751
Cholangitis	0	1 (5.9%)	0.232
Wound infection	0	4 (30.8%)	0.012
Perioperative death	0	0	

SIRS systemic inflammatory response syndrome

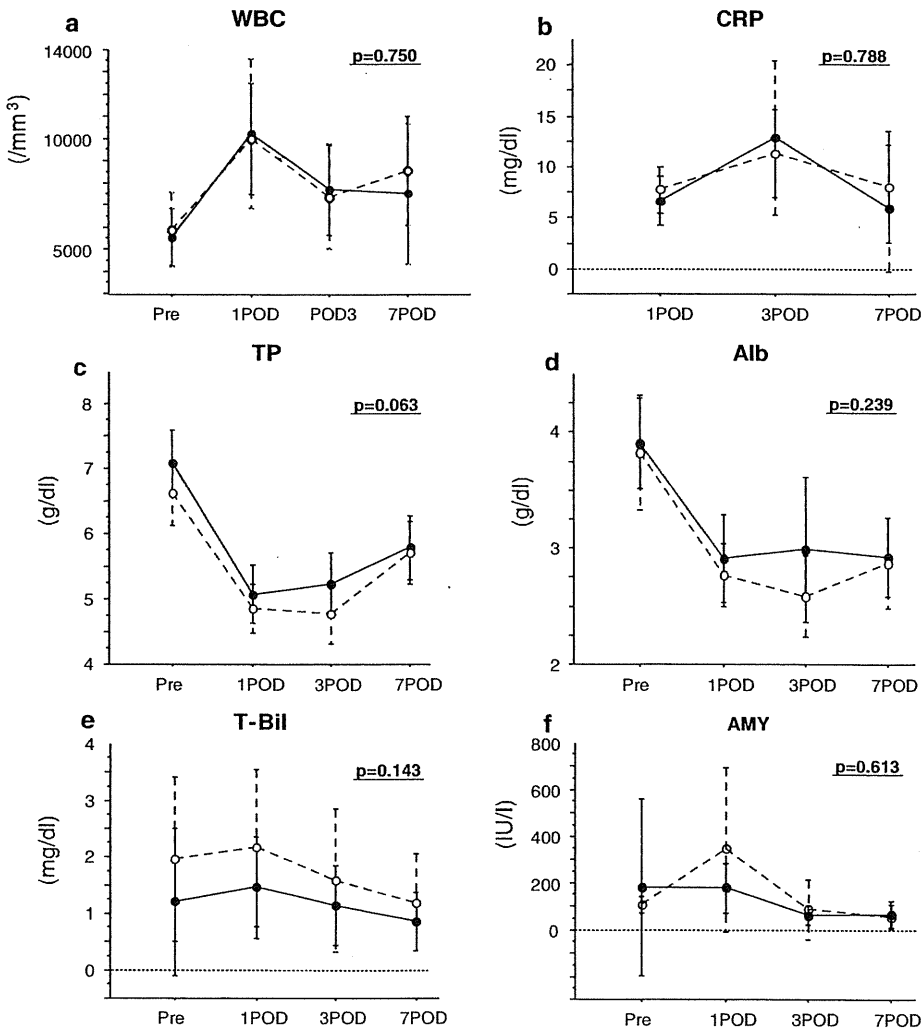

Fig. 1 Laboratory blood test results. *Filled circles* Impact group, *open circles* control group. **a** White blood cell count (*WBC*), **b** C-reactive protein (*CRP*), **c** total protein (*TP*), **d** serum albumin (*Alb*), **e** total bilirubin (*T-Bil*), **f** serum amylase (*AMY*), **g** glutamic oxaloacetic transaminase (*GOT*), **h** glutamic pyruvic transaminase (*GPT*), **i** blood urea nitrogen (*BUN*), **j** serum creatinine (*Cr*), **k** body weight (*BW*), **l** acute physiology and chronic health evaluation score II (*APACHE-II*)

not differ significantly between the two groups, the improvements in the gain or loss of BW after surgery showed a better course in the Impact group than in the control group. To evaluate the systemic severity of patients after surgery, we utilized the APACHE-II classification. A high postoperative APACHE-II score predicts an increased

Fig. 1 continued

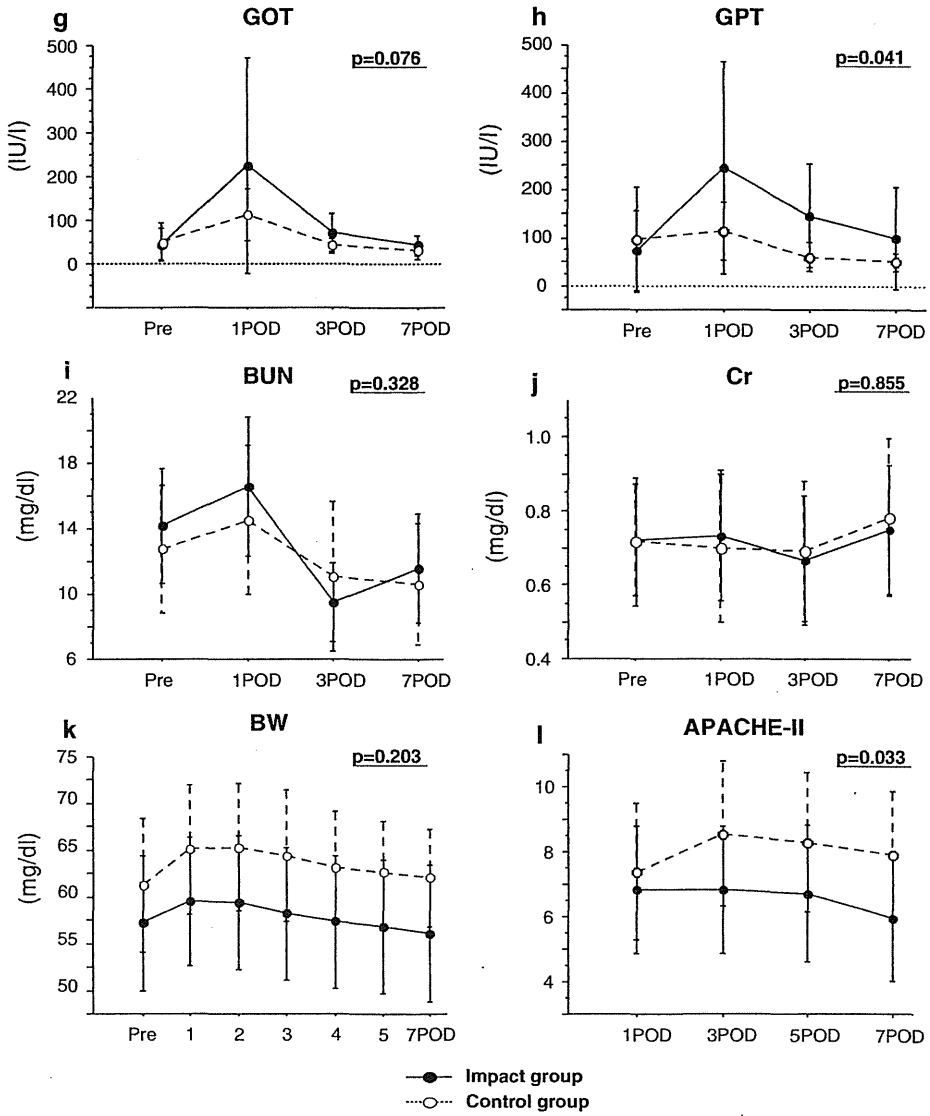

risk of a complicated postoperative course [33]. The change in the total APACHE-II score after PD was significantly lower in the Impact group than in the control group ($p = 0.033$). Among the factors measured for the APACHE-II scores, the following factors showed significantly lower scores in the Impact group than in the control group: temperature on POD 1 ($p = 0.008$), mean arterial pressure on POD 1 ($p = 0.048$), heart rate on POD 5 ($p = 0.019$) and POD 7 ($p = 0.049$), and hematocrit on POD 7 ($p = 0.006$).

Discussion

Preoperative oral supplementation with Impact (750 mL/day for 5 days) was well tolerated by patients scheduled to undergo PD. The compliance rate was more than 80%, and the duration and dose of Impact used in this study were suitable. This encouraging result suggests that Impact could also be ingested by outpatients prior to elective PD.

In the present series, one patient with IPMN could not tolerate Impact because of pancreatitis and cholangitis. This patient complained of epigastralgia, fever, and jaundice after beginning to consume Impact. The patient's laboratory data showed elevated serum amylase and bilirubin levels. We suspect that this patient's pancreatitis and cholangitis might have originated from an obstruction caused by a mucinous secretion from the primary tumor, because the pancreatitis and cholangitis occurred simultaneously and progressed synchronously. Actually, the elevated serum bilirubin level consisted predominantly of